Finger thickening during extra-heavy oil waterflooding: simulation and interpretation using pore-scale modelling

Regaieg M. (1), McDougall S.R. (1), Bondino I. (2), Hamon G. (2)
(1) Heriot Watt University, (2) Total E&P

This paper was prepared for presentation at the International Symposium of the Society of Core Analysts held in Avignon, France, 8-11 September, 2014

ABSTRACT

Although thermal methods have been popular and successfully applied in heavy oil recovery, they are often found to be uneconomic or impractical. Therefore, alternative production protocols are being actively pursued and an interesting option is water and/or polymer flooding.

Such a technique has been successfully tested in laboratory investigations, where oil recovery was found to be much higher than expected (paper SCA2011-18). Moreover, in some of the core scale experiments reported using 2D slabs of Bentheimer sandstone, X-ray scans performed during the flooding sequence provided evidence of an interesting new phenomenon – post breakthrough, highly dendritic water fingers were seen to thicken and coalesce, forming braided water channels and improving sweep efficiency. However, the causes of this behaviour are not clearly understood and the mechanisms governing such displacements consequently require further investigation.

To this end, we describe a new fully dynamic network model that has been developed to investigate finger thickening during water flooding of extra-heavy oils. The displacement physics has been implemented at the pore scale and, following a successful benchmarking exercise against numerous micromodel experiments, a range of slab-scale (30cm x 30cm) simulations has been carried out and compared with the corresponding experimental observations. We show that the model is able to replicate finger architectures similar to those observed in the experiments and go on to reproduce and interpret, for the first time to our knowledge, finger thickening following water breakthrough. Finally, we examine the impact of several parameters – core length, wettability and injection rate – on the finger swelling phenomenon.

Keywords: *viscous fingering, finger thickening, heavy oil, recovery, non-thermal, immiscible displacement*

INTRODUCTION

The recovery of heavy oil by water-flooding involves the displacement of a highly viscous fluid by one of much lower viscosity and this often results in the occurrence of so-called viscous fingering, which can be highly detrimental for oil recovery. The fingering causes early water breakthrough and, as a consequence, poor sweep efficiency. However, some recent laboratory studies have suggested that, under certain circumstances, water-flooding into extra-heavy oil (with viscosity up to 7000 cP) could actually result in higher than expected oil recovery (Bondino et al, 2011; Skauge et al, 2012; Skauge et al 2013). X-ray imaging of fluid fronts during these experiments has

highlighted a finger swelling mechanism that has not been previously reported and the causes of this behaviour – as well as the physics involved in such displacements – have not been explained to date. In this paper, we present a pore network modelling study that attempts to shed some light into this interesting phenomenon.

Over the past few decades, several studies have been undertaken to understand the mechanisms governing unsteady-state displacements. For instance, Lenormand *et al* (1988) carried out a large number of two phase drainage experiments covering a wide range of capillary numbers and viscosity ratios and pore network model simulations were also presented to help analyse the experimental results. However, their study was limited to behaviour up to breakthrough and their simulations were performed using relatively small networks. Several attempts to simulate viscous fingering using a continuum approach and fractal theory have also been reported in the literature (Bogoyavlenskiy, 2001; Chen *et al* 1988; Fernández and Albarrán, 1990; Løvoll *et al*, 2004; Oxaal, 1991; Paterson, 1984) but such macroscopic approaches are not able to adequately account for important pore scale mechanisms. An alternative mesoscopic approach was presented by Dong *et al* (2011) and this was successful in reproducing displacement experiments performed in Hele-Shaw cells and the effect of wettability on displacement pattern could be simulated. However, this model was unable to consider viscosity ratios beyond M=5.

In this paper we present a new dynamic drainage pore network model that builds upon an earlier model developed by McDougall and Sorbie (1993) in the context of unsteady-state displacements in laminated media. We begin here with a validation of the new model against a range of published experimental micromodel results and then go on to simulate laboratory-scale water-floods in large Bentheimer sandstone slabs (30cm x 30cm areal section). We are able to find a good qualitative agreement with the full range of observed displacement regimes, including finger thickening after breakthrough at highly adverse viscosity ratios. We stress here that no attempt has been made to history-match any of the experimental behaviours – once the model has been anchored using physical rock fabric parameters (PSD, connectivity distribution), the water-floods are simply initiated using the appropriate laboratory fluid data and experimental flow rates. Finally, we use our approach to study the effects of varying core length, rock wettability, and injection rate upon the finger swelling phenomenon.

EXPERIMENTAL SUMMARY

A number of experiments involving water and polymer injection into extra heavy oil have been performed recently using 30cm x 30cm x 2cm slabs of Bentheimer sandstone (precise details of the experimental procedures adopted can be found in Skauge et al, 2012). The Bentheimer slabs used in the study were relatively homogenous in nature, with a porosity of approximately 24% and permeability of around 2.5 Darcies, and were installed vertically into an X-ray scanner after having been sealed with epoxy resin. The densities of the oil and water were very close to one another and, as a consequence, the displacements were considered to be unaffected by gravitational instabilities.

Rail distributors were installed along the inlet and outlet edges of the slabs, with each rail having a central injection/production point and a groove to distribute the fluids across the entire inlet/outlet cross section. Each rock was dried at 80°C, vacuum saturated

with 7g/l NaCl brine and then oil was injected. The slab was subsequently aged for 3 weeks at 50°C. Two water injection experiments were reported: (i) experiment E7000, using 7000 cP oil with brine injected at the bottom of the slab, and (ii) experiment E2000, where 2000 cP oil was used and injection was performed from the top of the slab.

E7000 was characterised by an early water breakthrough after 0.04 PV injected, followed by a rapidly-increasing water-cut that reached 90% after 0.6 PV. After 2.3 PV injected, 20% of the OOIP had been recovered and, at the end of the waterflood (5.1 PV), this had increased to 26.4% – the water cut at this late stage was very high (~99%). Similar early water breakthrough behaviour was observed in the E2000 experiment (0.043 PV injected) but the oil recovery was substantially higher (28.5% of oil had been recovered after 2.3 PV injected versus 20% for E7000).

The displacement regime during the waterflooding was similar in both experiments (as inferred from X-ray data) and examples of the patterning from both experiments are shown in Figure 1. Initially, sharp viscous fingers were observed and these grew rapidly towards the outlet edge of the slab. The fingers appeared more dendritic in the E7000 experiment and some instabilities were seen to propagate faster than others, preventing the growth of some of the smaller fingers. Following water breakthrough, fingers throughout the slab appeared to thicken and coalesce, forming broad water channels and leading to an improvement in sweep efficiency. Finger thickening was found to be even more extensive in the E2000 experiment.

MODEL SUMMARY

Pore network modelling is now a well-established technique for the study of various pore scale phenomena that cannot be reproduced by conventional continuum-scale numerical simulators (see, for example, McDougall and Sorbie,1995; Valvatne and Blunt, 2004; Bondino et al, 2009, for details of the approach and various applications). The porous medium is modelled as a number of interconnected pore elements ("pores") representing the void space in the rock and the modelling framework is sufficiently flexible to allow the underlying network to be created using the statistical properties of a given rock – data having been obtained from rock CT images, for example. Multiphase flow models can then be developed and applied to this *in silico* network model.

Nodal Pressure Solution

Once the network has been constructed, solution of the pressure field for single-phase flow can be carried out straightforwardly through the application of mass conservation at each node. At every node *i* we can write:

$$\sum_{i,j} Q_{ij} = 0 \qquad (1)$$

where Q_{ij} is the flow rate from nodes i to j (calculated as $Q_{ij} = (P_i - P_j)G_{ij}$ where P_i is the nodal pressure at node i and G_{ij} is the conductance of the pore linking nodes i and j approximated by Poiseuille's law as $G_{ij} = \frac{\pi {R_{ij}}^4}{8\mu L_{ij}}$)

This leads to a set of linear pressure equations that can be solved numerically to yield the individual nodal pressures. However, in two phase flow, the flow within a pore

containing an interface separating wetting and nonwetting phases must account for the capillary pressure drop across that interface, and so we now have:

$$\begin{cases} Q_{ij} = G_{ij}(P_i - P_j + P_c) \text{ if } P_i - P_j > -P_c \\ Q_{ij} = 0 \; if \; P_i - P_j \leq -P_c \end{cases} \quad (2)$$

The capillary pressure is defined using Young-Laplace's law ($P_c = \frac{2\sigma cos\theta}{R}$), where σ is the interfacial tension, θ is the contact angle ($\theta = 180°$ for a strongly oil wet system) and R is the radius of the associated pore throat. It should be noticed that the capillary pressure is negative for an oil wet system. A matrix form of the problem can be constructed and is given by:

$$G * p = q_b + C_s q_c \quad (3)$$

where G is the conductance matrix, p is the pressure column vector – containing the nodal pressures in the network, C_s is the capillary scale defined as $C_s = \frac{2\sigma}{P_{inlet} L_s}$, q_b and q_c are respectively the column vector of boundary conditions – containing the local rates of the inlet pores, and the capillary effects column vector – representing the effect of capillary pressure drop at the fluids interface, P_{inlet} is the inlet pressure and L_s is the length scale (usually taken as the smallest radius in the network).We note that the second equation in (2) means that only the nonwetting invading phase can displace the defending wetting phase – we do not consider counter current imbibition events at this stage. Hence, pores having $P_i - P_j \leq -P_c$ are effectively "*closed"* pores.

However, simply solving the pressure field after setting the flow rate of such closed pores to zero is not as straightforward as it may initially appear. It is clear that ($P_i - P_j$) cannot be known before solving the pressure field and the pressure solution itself depends upon the distribution of closed pores selected, which in turn depends upon comparisons between capillary entry pressures and viscous pressure drops. The solution to this difficulty is as follows: (i) initially no pores are closed and the pressure field is calculated over the full network, (ii) pores satisfying the second condition in (2) based upon the calculated pressure distribution and capillary entry conditions are identified and closed, (iii) a new pressure field is calculated over the full network of open and closed pores, (iv) steps (ii)-(iii) are iterated until we obtain consistency between the pressure solution and the flowing network of open pores.

Coupling injection rate and inlet pressure

In 2-phase flow, the inlet pressure that will give the target injection rate is not known *a priori.* Furthermore, the relationship between the inlet pressure and the injection rate is no longer linear when capillary pressure is taken into account – the value of the inlet pressure now affects the distribution of pores that are available for displacement (i.e. open to flow). In order to address this issue, an iterative Secant Method was used to find P_{inlet} satisfying $Q(P_{inlet}) = Q_{target}$. At each iteration, we calculate the inlet pressure at the *kth* iteration from:

$$P_{inlet\ k+1} = P_{inlet\ k} - (P_{inlet\ k} - P_{inlet\ k-1}) \frac{(Q(P_{inlet\ k}) - Q_{target})}{(Q(P_{inlet\ k}) - Q(P_{inlet\ k-1}))} \quad (4)$$

Using this inlet value, the pressure field is then calculated, the corresponding rate is computed, closed pores are identified and their conductance is set to zero. The pressure is then re-solved under the new conditions. If newly closed/opened pores are identified, they are closed/opened and the pressure field is calculated once again – the procedure is repeated until all closed/open pores are identified and the simulated rate is consistent with the target injection rate. Note that this model is also able to reproduce variations in pressure drop across the system throughout the flooding process.

Multiple pore filling

The dynamic model also considers multiple pore filling and meniscus tracking. First, we loop through all pores situated at the interface between oil and water and, for every pore; a net driving pressure ΔP_{net} is calculated:

$$\Delta P_{net} = P_i - P_j + P_c \quad (5)$$

If the net driving pressure is positive, water will be able to displace oil within that pore and the time required to completely invade such a pore is computed as:

$$t = \frac{V_{pore}(1-S_w)}{\Delta P_{net} G_{ij}} \quad (6)$$

where S_w is the water saturation in that pore and V_{pore} is the total volume of the pore. The minimum filling time t_{min} over all pores in the network is identified, the pore having the shortest filling time is completely invaded with water, and menisci are updated in all other pores having $t > t_{min}$. The water saturation is then updated in each pore by:

$$S_{w\,new} = S_{w\,old} + \frac{t_{min} * \Delta P_{net} * G_{ij}}{V_{pore}} \quad (7)$$

VERIFYING THE MODEL AGAINST EXPERIMENTAL DATA

As a first test of the dynamic drainage model, a network was constructed to represent the micromodel experiments described in the groundbreaking paper of Lenormand *et al* (1988). The pore radii were reproduced stochastically from the reported experimental distributions and the experimental fluid properties and injection rates were used as inputs for the simulation. We stress here that there has been no attempt to history match the experimental observations – the inputs to the model were simply those reported in the published papers. We compared qualitatively our simulated invasion patterns against 35 experiments and a selection of the comparisons is shown in Figure 2 (a full set of comparisons can be found in Regaieg et al, 2014). In all cases, very good agreement was found with the experiments and all of the observed flow regimes were reproduced for a wide range of viscous ratios and capillary numbers. At low rates, an invasion percolation like pattern was obtained. This displacement is controlled by the capillary entry pressures of the pores at the interface and is characterised by invasions happening in all directions even towards the inlet in some cases. This leads to occurrence of loops that trap sometimes large quantities of oil. However, at high rates (and unfavourable mobility ratios) viscous fingering was observed. In this regime, tree shaped fingers are formed and grow towards the outlet leading to a very poor sweep efficiency. The invasion patterns in capillary and viscous dominated regimes are very different and can easily be identified from the saturation maps.

Although Lenormand experiments were performed nearly three decades ago, it appears that no published model has been able to reproduce the displacement regimes of

all the experiments reported in that paper. This gives us additional confidence in our *in-silico* approach.

FINGER THICKENING PHENOMENON

Slab scale simulations

A full scale series of simulations have been performed using rock/fluid data and injection protocols corresponding to those characterising the E7000 and E2000 experiments. We have restricted ourselves at present to large-scale 2D simulations in order to focus on finger morphology and development – consideration of the third dimension is conceptually straightforward but computationally expensive. A scaled injection rate was calculated in order to match the injection fluxes used in the 3D slab experiments (corresponding to a capillary number of 6.9E-9). The behaviour of the pressure drops in the simulations behaved in a similar way to those observed in the experiments – the differential pressures initially decreased as the water advanced towards the outlet but then began to stabilise after breakthrough (Figure 6)

Before breakthrough, the differential pressure was high in both E7000 and E2000 simulations and, as a consequence, viscous pressures were initially much higher than capillary pressures within the networks – sparse, directed fingers of invading water were the result (Figure 3). However, at water breakthrough, the pressure gradient across system-spanning fingers dropped sharply and the viscous pressure gradients acting across all associated pores decreased. Indeed, when we examine the pressure profile of E2000 more closely at breakthrough (Figure 4) we notice that the highest pressure gradients now occurred around the perimeters of fingers situated upstream of the outlet face of the network. This not only accelerated the growth of these fingers towards the outlet but also caused some degree of finger thickening. This is confirmed by Figure 5, which represents the water invasions after breakthrough at different stages of the E2000 simulation. In fact, Figure 5 represents the change between the saturation map at the breakthrough and later stages of the simulation. We can clearly see that the new water invasions were occurring primarily around the tip of previous instabilities that had not yet reached the outlet. After several fingers reached the outlet, the inlet pressure dropped further and reached a plateau. At this stage of the water-flood, the viscous pressures which were driving the water towards the outlet became even smaller. This led to increasing the impact of the capillary forces on the displacements and pores having a lower capillary resistance were more likely to be filled first. Thus, water began to spread in all directions – the fingers thickened further and broad channels emerged as a result of coalescing fingers.

The slab scale simulations performed using our dynamic model exhibited fingering behaviours that are very similar to those observed in the experiments. Initially, several sharp fingers were formed near the inlet and progressively some of them grew faster than the others inhibiting the development of the shorter ones. These instabilities had a leaf like shape and were oriented in the direction of the outlet. Furthermore, the thickening phenomenon evident from the X-ray scans could also be reproduced by the simulator. We note that, whilst differences were observed between the simulated and experimental differential pressures before the plateau stage – due mainly to the difference in dimensionality between the 2D networks and 3D experiments – the plateau value of

the differential pressure drop generated by the model matched the experimental data extremely well (Figure 6). Of course, we should not expect to reproduce fingers in identical spatial locations (our network is constructed stochastically) and we should also bear in mind that the X-ray data are essentially 2D composites of 3D scans. Nevertheless, given the relatively simple modelling approach adopted here, our model performs well against the available experimental data by simulating the behaviour of instabilities before the BT and by reproducing the finger swelling phenomenon. This allows us to present a hypothesis of why finger thickening is observed experimentally post water breakthrough. We propose that this phenomenon is caused by a drop in differential pressure through sample-spanning fingers after breakthrough, resulting in the highest local pressure gradients after breakthrough being primarily associated with the tips of upstream fingers that have not yet reached the outlet. This makes the flow less viscous dominated resulting in an increasing impact of capillary forces which leads to fingers growth in all directions.

Having applied the model using experimental data, we now go on to examine the impact of varying a number of system variables on finger development and thickening. In order to reduce computational runtimes, we choose to use 5cm x 30cm simulations corresponding to 250*1500 network for these sensitivities.

Impact of system variables on finger development and thickening

a- Core length

Our first sensitivity focuses on system length and several simulations were performed to investigate the effect of core length on the finger thickening behaviour. The experimental conditions of E7000 were used (using a scaled injection rate of Q= 0.005 cc/hr that matched the experimental flux) and a weakly oil wet condition was assumed throughout (θ=100º). For network lengths equal to 30 cm and 15 cm, finger thickening was clearly observed (Figure 8) and the plateau differential pressure post water breakthrough remained higher than the mean capillary entry pressure characterising the underlying network for the duration of the flood (Figure 7) and which is calculated using Young-Laplace's law as $P_c = \frac{2\sigma cos\theta}{\bar{R}}$ where $\bar{R}$ is the mean pore radius in the network.

For a system length equal to 7.5 cm, the pressure drop reached a plateau value very close to the mean capillary entry pressure of the network up until 4.5 PV injection. During this time, the perimeter pores of upstream fingers began to thicken and grow until reaching the outlet. When a second finger reached the outlet, the pressure drop decreased further, falling below the mean capillary entry pressure in the network – shortly after this second pressure reduction, finger swelling ended. An even shorter network (3.25 cm) exhibited interesting behaviour. In this case, the differential pressure fell below the mean capillary entry pressure in the network once the water reached the outlet. In this case, no finger thickening behaviour was observed.

These results show that finger thickening occurs when the pressure drop at the plateau stage is higher than the mean capillary entry pressure. As a consequence, this suggests that the length of the core is an essential parameter for the finger thickening phenomenon. In fact, short cores may not be able to maintain a differential pressure high enough to cause finger swelling. Furthermore, the longer the core, the higher the differential pressure required to maintain a fixed injection rate – consequently, for long

cores, the pressure drop at the plateau stage is more likely to be higher than the mean capillary entry pressure and finger thickening more likely to occur.

b- Wettability

Simulations were performed using the experimental conditions of E7000 (Q= 0.005 cc/hr) under two different wettability scenarios: a strongly oil-wet case (θ=170°) and a weakly oil-wet case (θ=100°). The stabilised value of the pressure drop corresponding to the strongly oil-wet case was found to be lower than the mean capillary entry pressure in the network, while for the weakly oil-wet case the opposite was the true (Figure 9). We find that finger thickening is predicted only for the weakly oil-wet case (Figure 10) – for the strongly oil-wet case, the saturation path did not change after water breakthrough. This can be explained as follows: a lower contact angle reduces the mean capillary entry pressure in the network and, as a consequence, the differential pressure now lies above this value and so capillary entry criteria can still be satisfied. These results again show that, to have finger thickening, the pressure drop across the system at the plateau stage of the flood should be higher than the average capillary pressure in the network.

c- Injection Rate

Two simulations were performed using the rock/fluid conditions of E7000 at two different injection rates Q_1=0.005 cc/hr and Q_2=0.05 cc/hr (note that the scaled experimental rate corresponds to Q=0.005 cc/hr). The wettability scenario considered was a strongly oil-wet case (θ=170°). We find that the simulated pressure drop for the low rate simulation fell below the mean capillary entry pressure in the network (Figure 11), whereas for the high rate it remained higher than the mean capillary entry pressure throughout. Figure 12 shows that the phenomenon of finger thickening only occurred during the high rate simulation, in line with our earlier hypothesis.

CONCLUSIONS

A fully dynamic pore network model has been presented that includes an iterative approach to enable capillary pressure to be taken into account when solving for the global pressure field. In addition, we include a time-dependent pressure drop in the formulation that allows us to model fixed injection rate experiments reported in the literature.

The model has been used to qualitatively reproduce slab scale waterflooding into extra heavy oil experiments. Before breakthrough, dendritic viscous fingers were obtained, whilst after breakthrough the instabilities began to thicken and merge forming water channels. This behaviour is qualitatively similar to that observed in the laboratory studies.

We propose that the finger thickening behaviour is due to a rapid change in pressure drop after breakthrough and to the fact that the highest pressure gradients after breakthrough are found primarily at the tip of the upstream fingers. We suggest that the pressure drop at the plateau stage of the flood should be higher than the mean capillary entry pressure characterising the sample to have this phenomenon.

Finally, we indicate that core length, wettability and injection rate, are all important parameters affecting the finger thickening behaviour. Indeed, increasing the length of the

core, using a higher injection rate and/or having a more neutral wet condition all increase the potential of finger swelling and improved recovery.

ACKNOWLEDGEMENTS

The authors would like to thank Total E&P for their financial support, technical assistance and permission to publish the paper.

REFERENCES

1. Bondino I., Nguyen R., Hamon G., Ormehaug P. A., Skauge A., Jouenne S. (2011), Tertiary polymer flooding in extra-heavy oil: an investigation using 1D and 2D experiments, core scale simulation and pore-scale network models," reviewed proceedings for the 25th International Symposium of the Society of Core Analysts, Austin, Texas, USA, 18th to 21st September 2011
2. Bondino, I., McDougall, S. R., Hamon, G. (2009). Pore-Scale Modelling of the Effect of Viscous Pressure Gradients During Heavy Oil Depletion Experiments. Petroleum Society of Canada.
3. Bogoyavlenskiy, V. A. (2001). Mean-field diffusion-limited aggregation: A "density" model for viscous fingering phenomena. Physical Review E, 64(6), 066303.
4. Chen, J.-D., Dias, M. M., Patz, S., & Schwartz, L. M. (1988). Magnetic Resonance Imaging of Immiscible-Fluid Displacement in Porous Media. Physical Review Letters, 61(13), 1489-1492.
5. Dong, B., Yan, Y. Y., & Li, W. Z. (2011). LBM Simulation of Viscous Fingering Phenomenon in Immiscible Displacement of Two Fluids in Porous Media. Transport in Porous Media, 88(2), 293-314.
6. Fernández, J. F., & Albarrán, J. M. (1990). Diffusion-limited aggregation with surface tension: Scaling of viscous fingering. Physical Review Letters, 64(18), 2133-2136.
7. Lenormand, R., Touboul, E., & Zarcone, C. (1988). Numerical Models and Experiments On Immiscible Displacements In Porous Media. Journal of Fluid Mechanics, 189, 165-187
8. Løvoll, G., Méheust, Y., Toussaint, R., Schmittbuhl, J., & Måløy, K. J. (2004). Growth activity during fingering in a porous Hele-Shaw cell. Physical Review E, 70(2), 026301.
9. McDougall, S. R., & Sorbie, K. S. (1993). The Combined Effect of Capillary and Viscous Forces on Waterflood Displacement Efficiency in Finely Laminated Porous Media. Paper presented at the SPE Annual Technical Conference and Exhibition, Houston, Texas.
10. McDougall, S. R., & Sorbie, K. S. (1995). The Impact of Wettability on Waterflooding: Pore-Scale Simulation. Society of Petroleum Engineers.
11. Oxaal, U. (1991). Fractal viscous fingering in inhomogeneous porous models. Physical Review A
12. Paterson, L. (1984). Diffusion-Limited Aggregation and Two-Fluid Displacements in Porous Media. Physical Review Letters, 52(18), 1621-1624.
13. Regaieg, M., McDougall, S.R., Hamon, G.(2014). Non-thermal heavy oil production: A Pore-to-core approach to investigate the impact of wettability during cold water injection into heavy oils. Paper presented at the World Heavy Oil Congress , New Orleans, Louisiana, USA.
14. Skauge, A., Ormehaug, P. A., Gurholt, T., Vik, B., Bondino, I., & Hamon, G. (2012). 2-D Visualisation of Unstable Waterflood and Polymer Flood for Displacement of Heavy Oil. Paper presented at the SPE Improved Oil Recovery Symposium, Tulsa, Oklahoma, USA.
15. Skauge, A., Ormehaug, P. A., Vik, B., Fabbri, C., Bondino, I., Hamon, G. (2013). Polymer Flood Design for Displacement of Heavy Oil Analaysed by 2D-imaging. Paper presented at the 17th European Symposium on Improved Oil Recovery, St.Petersburg, Russia.
16. P H Valvatne and M J Blunt, (2004) "Predictive pore-scale modeling of two-phase flow in mixed wet media," Water Resources Research, 40, W07406.

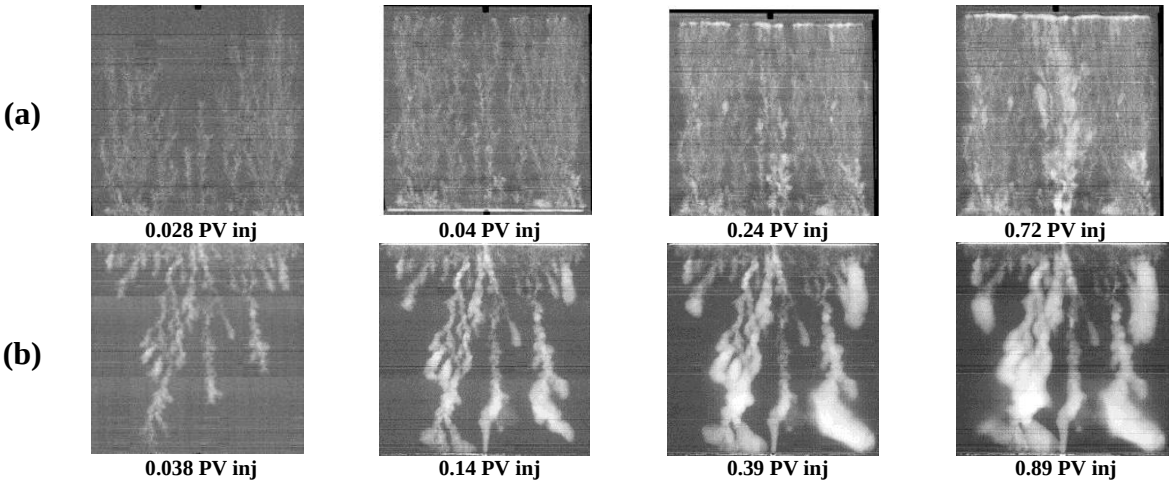

Figure 1: X-ray images of Waterflooding into Bentheimer in experiments E7000 where water was injected from the bottom (a) and E2000 where the water was injected from the top (b) (Skauge et al, 2012)

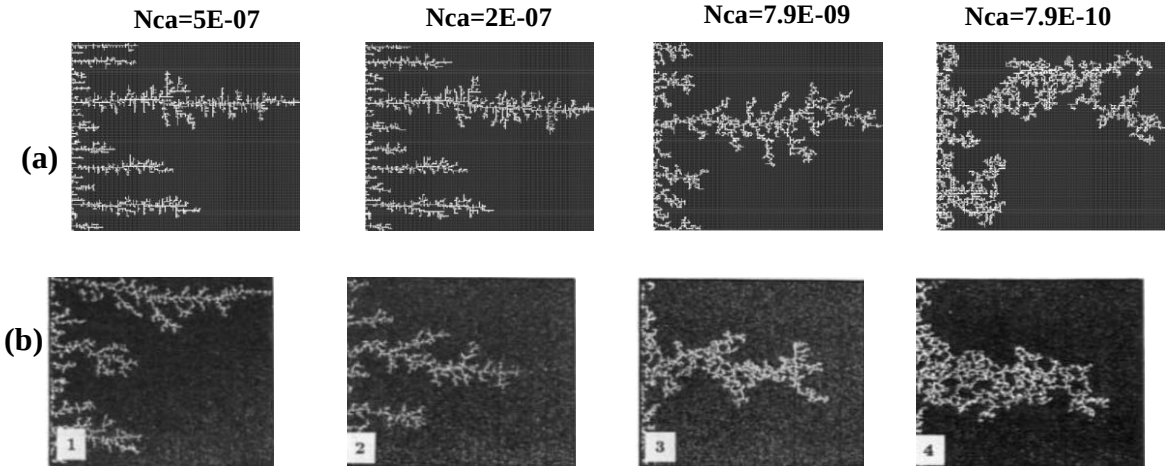

Figure 2: Comparison between simulations (a) and experiments (b) of Air (white) displacing heavy oil (M=55555)at BT.

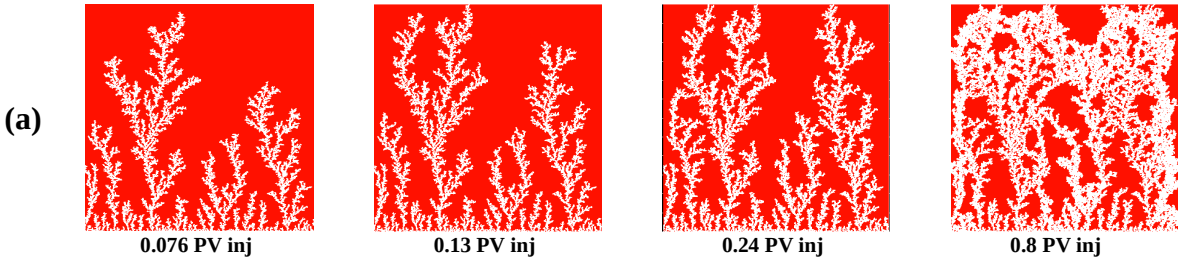

(b)

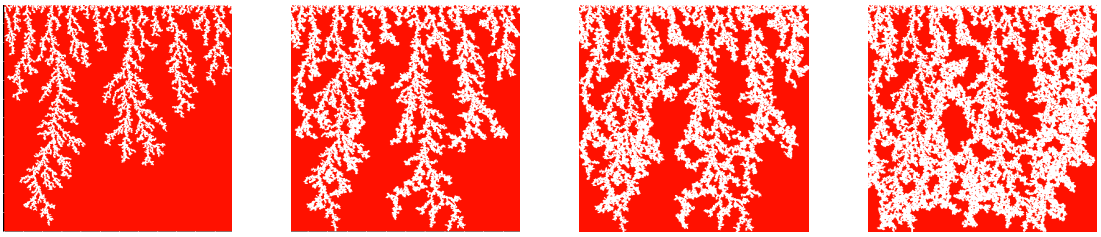

0.076 PV inj **0.2 PV inj** **0.32 PV inj** **0.88 PV inj**

Figure 3: Simulation of E7000 (a) and E2000 (b) experiments

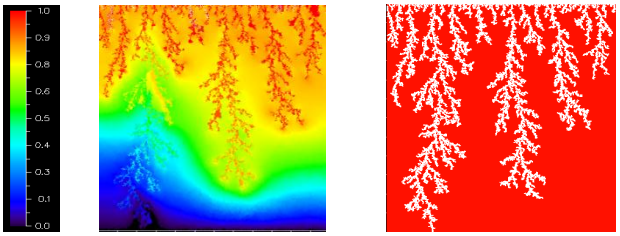

(a) **(b)**

Figure 4: Pressure of the *resident* fluid in each pore (a) and the saturation path (b) in E2000 simulation at BT. Note that some pores contain water and some pores contain oil – the pressures shown here correspond to the pressure within the resident fluid.

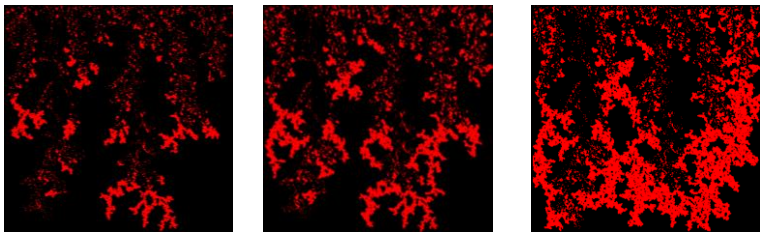

0.2 PV inj **0.32 PV inj** **0.88 PV inj**

Figure 5: Location of the new water invasions occurred after BT (red) at different stages of the simulation of experiment E2000

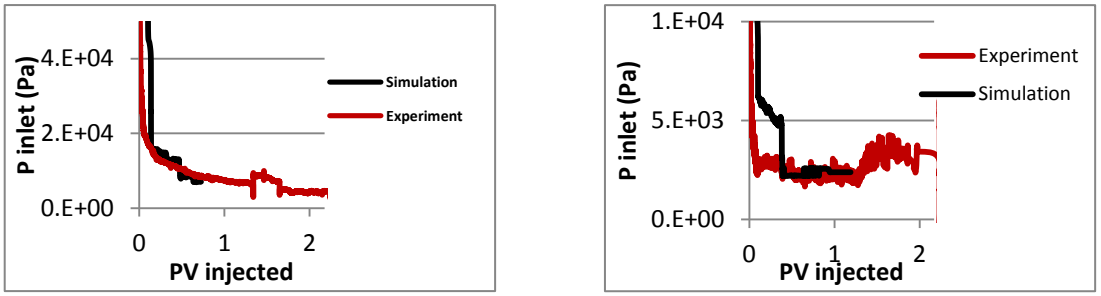

(a) (b)

Figure 6: Comparison between the simulated and measured differential pressure at the plateau stage in experiments E7000 (a) and E2000 (b)

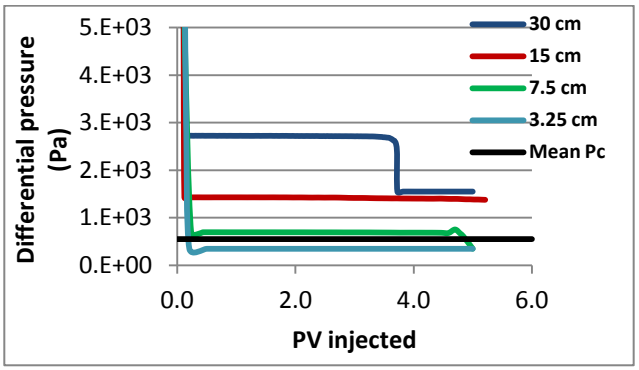

Figure 7: The differential pressure simulated for different networks lengths and the Mean Pc in the network (calculated using Young-Laplace's law and the average pore radius in the network). In this set of simulations: Q=0.005 cc/hr , Nca= 6.9 E-09, theta=100° and μoil=7000 cP.

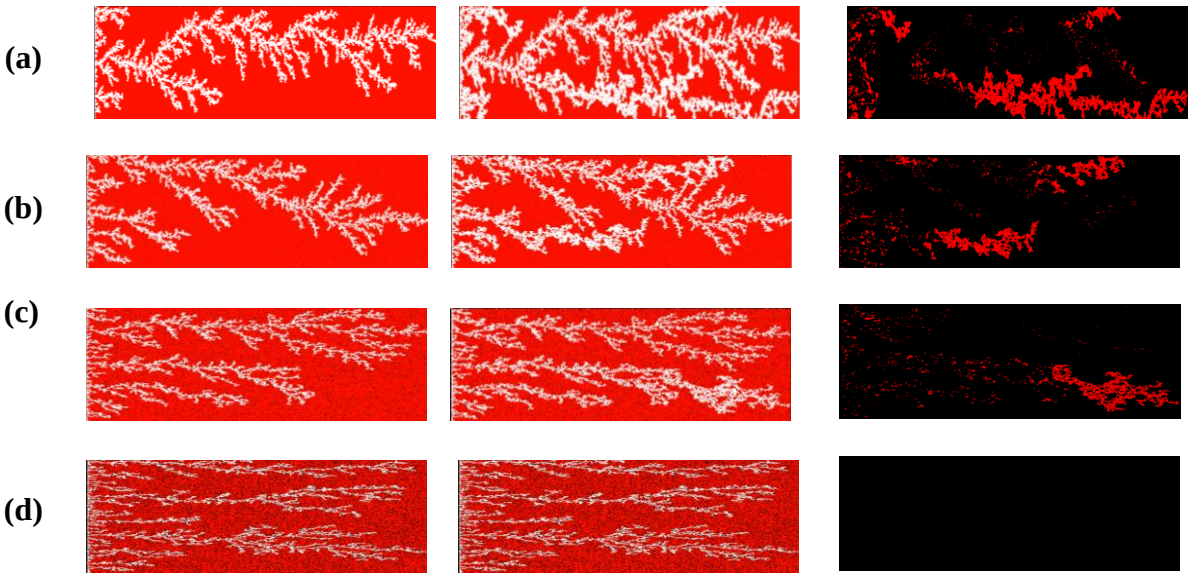

Figure 8: The saturation path at BT, the saturation path after BT(5PV) and the water invasions occurred after BT(5PV) for simulations with different network lengths: 30cm (a), 15 cm (b),7.5 cm (c) 3.25 cm (d). In this set of simulations: Q=0.005 cc/hr , Nca= 6.9 E-09 and theta=100° and μoil=7000 cP .

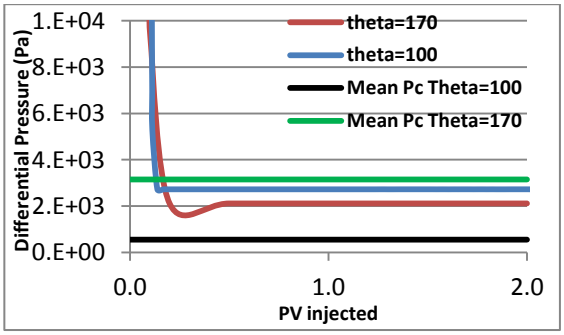

Figure 9: Comparison between the differential pressures in two simulations with different contact angles: theta=100 (blue) and theta=170 (red).The Mean Pc in the network (calculated using Young-Laplace's law and the Mean pore Radius in the network) In this set of simulations: Q=0.005 cc/hr, Nca= 6.9 E-09 and L=30 cm.

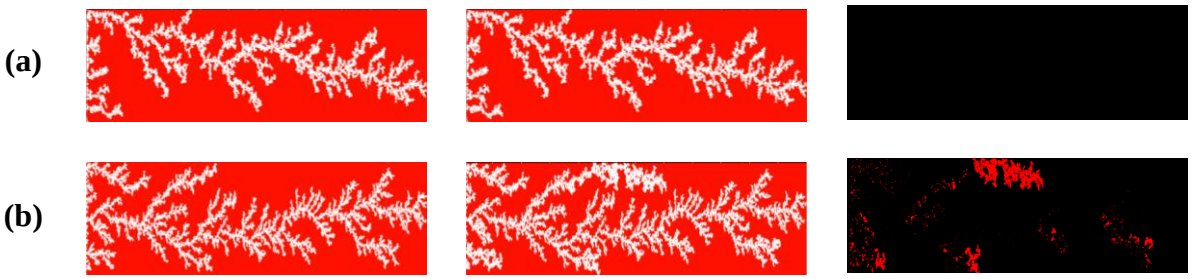

Figure 10: The saturation path at BT, the saturation path after BT (2 PV) and the water invasions occurred after BT(2 PV) for simulations with different contact angles theta=170 (a) and theta=100 (b). In this set of simulations: Q=0.005cc/hr, Nca= 6.9 E-09, L=30 cm and μoil=7000 cP.

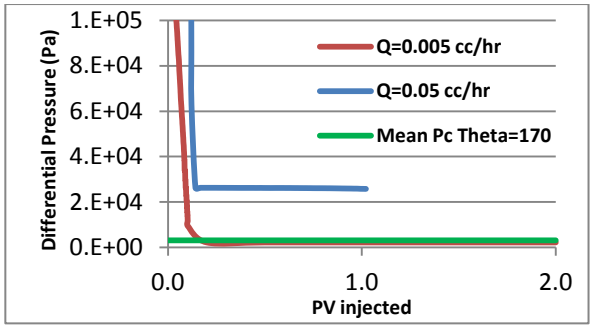

Figure 11: Comparison between the differential pressures in two simulations with different injection rates: Q=0.005 cc/hr (a) and Q=0.05 cc/hr. The Mean Pc was calculated using the average pore radius in the network. In these simulations theta=170 and L=30 cm.

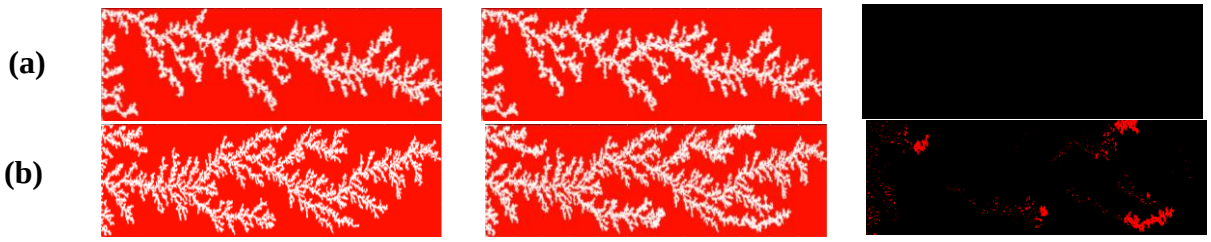

Figure 12: The saturation path at BT, the saturation path after BT (1 PV) and the water invasions occurred after BT (1 PV) for simulations with different injection rates: Q=0.005 cc/hr (a) and Q=0.05 cc/hr. In these simulations theta=170°, L=30 cm and μoil=7000 cP.